Journal of Magnetic Resonance 305 (2019) 146–151

Contents lists available at ScienceDirect

Journal of Magnetic Resonance

journal homepage: www.elsevier.com/locate/jmr

Heteronuclear NMR spectroscopy of proteins encapsulated in cubic phase lipids

Thomas G. Meikle [a], Ashish Sethi [b,c], David W. Keizer [c], Jeffrey J. Babon [d,e], Frances Separovic [c,f], Paul R. Gooley [b,c], Charlotte E. Conn [a], Shenggen Yao [c,*]

[a] School of Science, College of Science, Engineering and Health, RMIT University, Melbourne, VIC 3000, Australia
[b] Department of Biochemistry & Molecular Biology, The University of Melbourne, VIC 3010, Australia
[c] Bio21 Molecular Science and Biotechnology Institute, The University of Melbourne, VIC 3010, Australia
[d] The Walter and Eliza Hall Institute of Medical Research, Parkville, VIC 3052, Australia
[e] Department of Medical Biology, The University of Melbourne, VIC 3010, Australia
[f] School of Chemistry, The University of Melbourne, VIC 3010, Australia

ARTICLE INFO

Article history:
Received 3 May 2019
Revised 24 June 2019
Accepted 29 June 2019
Available online 1 July 2019

Keywords:
Heteronuclear NMR spectroscopy
Lipidic cubic phase
Protein hydration
Sensitivity enhancement
Solvent exchange

ABSTRACT

Lipidic cubic phases, which form spontaneously via the self-assembly of certain lipids in an aqueous environment, are highly prospective nanomaterials with applications in membrane protein X-ray crystallography and drug delivery. Here we report ^{1}H-^{15}N heteronuclear single/multiple quantum coherence (HSQC, HMQC) spectra of ^{15}N-enriched proteins encapsulated in inverse bicontinuous lipidic cubic phases obtained on a standard commercial high resolution NMR spectrometer at ambient temperature. ^{15}N-enriched proteins encapsulated in this lipidic cubic phase show: (i) no significant changes in tertiary structure, (ii) significantly reduced solvent chemical exchange of backbone amides, which potentially provides a novel concept for quantifying residue-specific hydration; and (iii) improved spectral sensitivity achieved with band-selective excitation short-transient (BEST) spectroscopy, which is attributed to the presence of an abundant source of ^{1}H nuclear spins originating from the lipid component of the cubic phase.

1. Introduction

Interactions between water and biomolecules, specifically protein hydration dynamics, play a critical role in the function of all biological systems [1]. However, advances in the experimental quantification of such effects, at least at the atomic level, have been slow. Solution NMR has been long considered as the leading means for gaining insight into site-specific protein hydration dynamics via measurement of the nuclear Overhauser effect (NOE) between water and proteins [2]. Nevertheless, quantification of protein hydration dynamics in aqueous solution (commonly employed for structural, interaction and dynamics studies) *via* the measurement of intermolecular NOE has proved challenging due largely to the presence of excessive bulk water molecules outside the hydration layer, which contribute to experimentally measured intermolecular NOE though long range dipole-dipole coupling [3].

Recently, it has been demonstrated that comprehensive residue-specific hydration dynamics measurements can be achieved *via* the use of reverse micelles [4,5]. Encapsulation of proteins in the aqueous centre of reverse micelles effectively eliminates the excessive bulk water around the proteins of interest and thus significantly reduces hydrogen exchange chemistry and considerably slows down the rapid water dynamics normally present in aqueous solutions [6]. Together with the use of relatively short mixing times, which limits the maximum NOE-detected distance to approximately 5 Å, NOE interactions observed between water and protein could be unequivocally assigned to the water molecules within the hydration layer [3,4].

Lipidic inverse bicontinuous cubic phases are a group of closely related structures formed by the spontaneous self-assembly of particular lipids in an aqueous environment. They consist of a single lipid bilayer, which approximates the geometry of a triply periodic minimal surface, resulting in the formation of two unconnected but interpenetrating networks of water channels. In binary lipid-water systems, three lipidic cubic phase (LCP) structures are observed experimentally: the diamond (Q_{II}^{D}), primitive (Q_{II}^{P}) and gyroid (Q_{II}^{G}), corresponding to space groups *Pn3m*, *Im3m* and *Ia3d*, respectively. [7] A three-dimensional schematic representation of

* Corresponding author.
E-mail address: shyao@unimelb.edu.au (S. Yao).

https://doi.org/10.1016/j.jmr.2019.06.017
1090-7807/

the Q_{II}^{D} LCP used in the present study, together with ^{15}N-labelled B1 immunoglobulin-binding domain of Streptococcal protein (GB1) encapsulation, and NMR sample setup are shown in Fig. 1. The ability of these materials to encapsulate hydrophilic compounds within the water channels, as well as amphiphilic and hydrophobic compounds within their membrane mimetic bilayer environment, has led to their increasing use in a number of fields, including the crystallization of membrane proteins (*in meso* crystallization) [8] and the encapsulation and delivery of therapeutic compounds [9–11]. Importantly, the geometry of these materials, including the water channel diameter, is highly tuneable *via* modifications to their lipid composition [12,13]. The compatibility and stability of the LCP under the various buffer and experimental conditions necessary for structural/dynamics studies, including temperature, pH, chemical reagents and detergents, have been well characterised [14–17].

Herein we describe a novel technique for achieving comparable exclusion of surrounding bulk water in aqueous protein solutions *via* their encapsulation within a lipidic inverse bicontinuous cubic phase matrix. We first report ^{1}H-^{15}N heteronuclear single/multiple quantum coherence (HSQC, HMQC) spectra of ^{15}N-enriched protein encapsulated in a LCP obtained using a standard commercial high-resolution NMR spectrometer at ambient temperature. Then we show experimental confirmation of reduced solvent chemical exchange of protein backbone amides in LCP encapsulation, analogous to those previously reported in reverse micelle encapsulated proteins. Protein encapsulation in LCPs thus provides a potential novel alternative to reverse micelles for quantitation of residue-specific protein hydration dynamics [4,5]. Finally, we demonstrate that additional spectral sensitivity gain can be achieved with the use of band-selective excitation short-transient (BEST) ^{1}H-^{15}N HMQC spectroscopy, attributed to the presence of abundant ^{1}H nuclear spins originating from the high lipid content of the LPC.

2. Results and discussion

A sample consisting of the ^{15}N-labelled GB1 encapsulated in a Q_{II}^{D} LCP was prepared by mixing lipid (monoolein, 62% w/w) and aqueous GB1 solution (38% w/w), resulting in the spontaneous formation of the LCP. The solubilized GB1 was thus encapsulated within the water channels, which at this level of hydration span approximately 4.5 nm in diameter (illustrated in Fig. 1b) [18]. The viscous LCP was then dispensed into a capillary, sealed and placed into a standard 5-mm NMR tube filled with $^{2}H_2O$ (illustrated in Fig. 1c and in Fig. S1, Supplementary Material). It is worth noting that, due to the high lipid content of the sample (62% w/w) and the small size of the capillary, 30 μL of protein solution is sufficient to form an adequate volume of LCP in this experimental setting. The resultant one dimensional ^{1}H spectrum of this LCP sample is shown in Fig. 2. The broad appearance of the 1D ^{1}H spectrum closely resembles that of a previously reported ^{1}H spectrum of a monoolein (Q_{II}^{G}) LCP in the absence of protein [19]. In both spectra the dynamic range is completely dominated by resonances in the upfield aliphatic region arising from the high lipid content. Similarly, in both cases the water within the LCP gives rise to a peak ca. 0.08 ppm downfield to that of the HDO signal, which arises from the surrounding $^{2}H_2O$ used for locking to the magnetic field (4.77 ppm, referenced to the internal reference, DSS, at 0.00 ppm). This downfield shift of the water resonance within the LCP has been attributed to changes in bulk magnetic susceptibility compared to aqueous solutions [19].

^{1}H-^{15}N HSQC spectra of GB1 both in aqueous solution and encapsulated in the monoolein LCP were recorded, with an overlay of the two spectra shown in Fig. 3a. A ^{1}H-^{15}N HSQC spectrum of GB1 in aqueous solution with full assignment of peaks can be found in Supplementary Material (Fig. S2). The ^{1}H-^{15}N HSQC of GB1 encapsulated in LCP resembles that in aqueous solution remarkably well. A nearly uniform downfield shift, ca 0.1 ppm along the ^{1}H dimension is clearly evident, and is in agreement with the downfield shift observed for the water signal in the LCP. Comparison of the GB1 ^{1}H and ^{15}N amide chemical shifts, in aqueous solution and encapsulated within the LCP, are shown in Fig. 3b and c, which demonstrate excellent linear correlations of chemical shifts between the two samples for both nuclei. The uniformity of the chemical shift differences observed between GB1 in LCP and aqueous solution confirms that encapsulation within the LCP does not induce significant changes to the tertiary structure of the protein. Another feature of the ^{1}H-^{15}N HSQC spectrum in LCP is the significantly broadened linewidth of resonances along the entire ^{1}H dimension. The increase in linewidth is not completely surprising, given the confined nature of protein encapsulated in LCP. Confinement conceivably hinders the rotational dynamics of the protein to some extent depending on the size of the protein under investigation and channel geometry of the LCP used. The abundance of proton nuclear spins originating from the lipid, would provide an additional source of proton dipole-dipole coupling through the mechanism of spin diffusion further leading to an increase in linewidth [20]. Consequently, this line broadening may be alleviated when partially or completely deuterated lipids are used for the formation of the cubic phase, as deuterated lipids would effectively eliminate many ^{1}H relaxation pathways contributing to this line broadening [21]. Finally, it is worth pointing

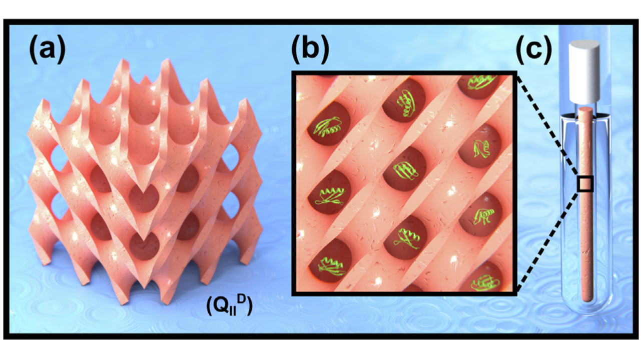

Fig. 1. (a) A three-dimensional representation of the Q_{II}^{D} LCP, (b) an illustration showing the encapsulation of GB1 protein within the water channels of the LCP, and (c) the experimental setup employing an LCP filled capillary sitting in a $^{2}H_2O$ filled NMR tube. A detailed view of (c) is presented in the Supplementary Material, Fig. S1.

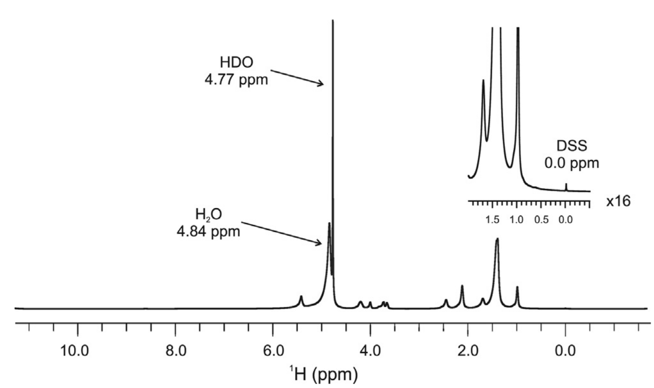

Fig. 2. One-dimensional ^{1}H spectrum of ^{15}N-labelled B1 immunoglobulin-binding domain of Streptococcal protein (GB1) encapsulated in monoolein (62% w/w) LCP. The *right inset* shows an expanded partial spectrum (from −0.5 to 2.0 ppm) with DSS (4,4-dimethyl-4-silapentane-1-sulfonic acid) signal used for reference indicated. The total volume of GB1 solution encapsulated in cubic phase is ca. 30 μL.

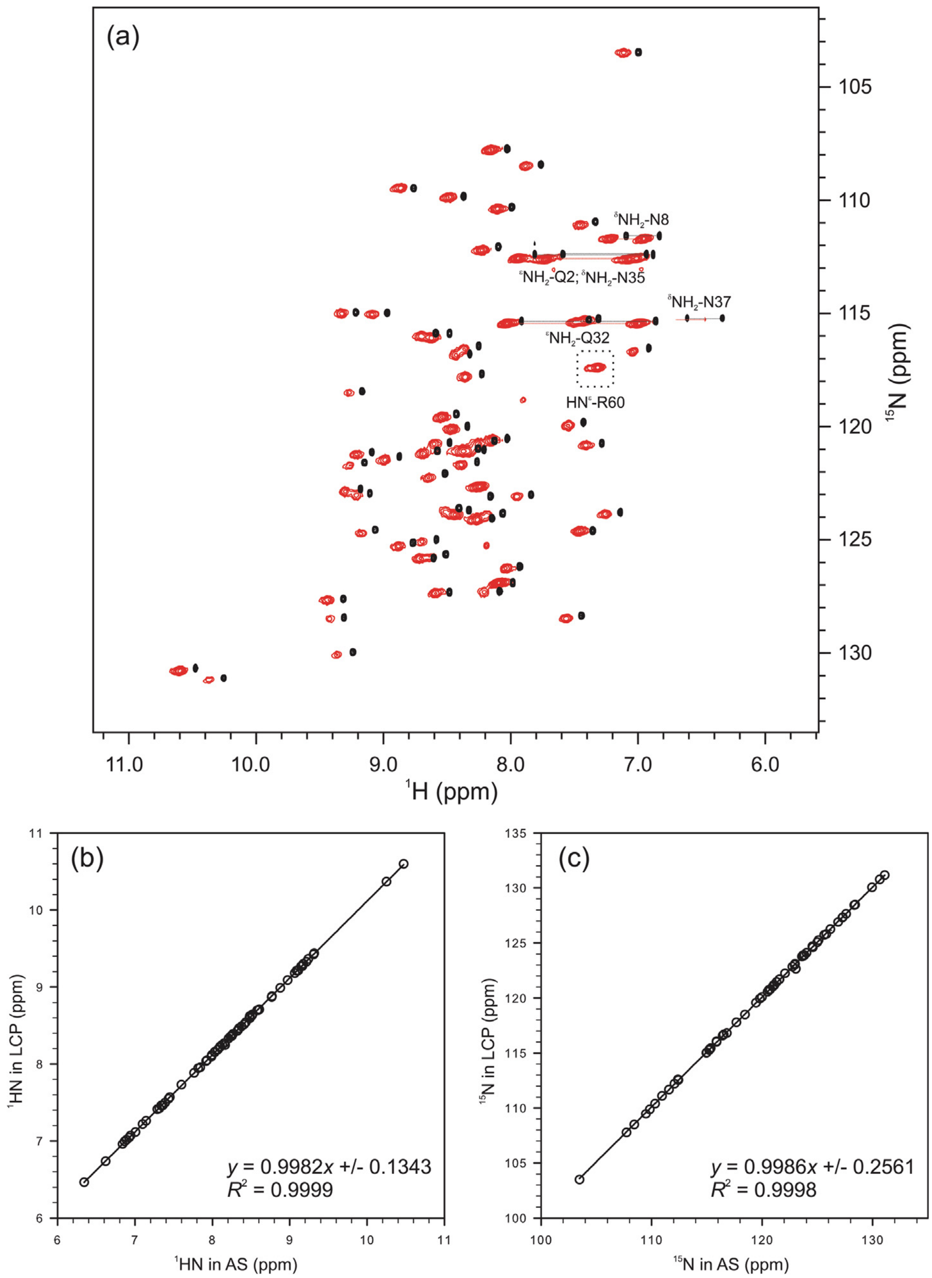

Fig. 3. Comparison of ^{1}H-^{15}N HSQC spectra of GB1 in aqueous solution and in lipidic cubic phase. (a) Overlay of ^{1}H-^{15}N HSQC spectra of GB1 in aqueous solution (in black, 0.35 mM, ca. 550 μL, in a standard 5-mm NMR sample tube), and in LCP (in red, 62% w/w monoolein, 38% w/w aqueous GB1 at 1.8 mM, loaded into a 2-mm capillary). Sidechain resonances arising from Asn and Gln residues are indicated by dashed lines (also see Fig. S2, Supplemental Materials). The folded peak arising from the sidechain amide of R60 is indicated with a dashed-box. Both spectra were acquired and processed with identical parameters except the number of scans used for signal averaging (NS = 8 and 64 for aqueous solution and LPC, respectively, corresponding to a total acquisition times of 20 min and 2 h 40 min); and (b, c) Plots of amide ^{1}H and ^{15}N chemical shifts of GB1 in LCP versus those in aqueous solution (AS) showing that downfield shift of both ^{1}H and ^{15}N chemical shifts were uniform across the entire molecule with slopes of linear regression for both graphs being 0.998 and 0.999 for ^{1}H and ^{15}N, respectively. (For interpretation of the references to colour in this figure legend, the reader is referred to the web version of this article.)

out that the folded sidechain NH of Arg60 (with a ^{15}N chemical shift of 85 ppm in an unfolded ^{1}H-^{15}N HSQC spectrum, which usually undergoes extremely fast exchange with solvent water, preventing its detection in the conventional ^{1}H-^{15}N HSQC spectrum) gave rise to a normal-looking peak in the LCP sample (indicated by a dashed-box in Fig. 3a). This effect is primarily due to a substantial reduction in bulk water around the protein after encapsulation in the LCP, and the resultant reduction in the rate of hydrogen exchange (see below).

Given the similar geometric dimensions of the LCP water channels (ca. 4.5 nm diameter) and the aqueous centre of reverse micelles in comparable experiments, similar elimination of the excessive bulk water around the proteins can be assumed. We thus expect the rate of hydrogen exchange of protein backbone amides in the LCP sample to be significantly reduced, which was confirmed *via* CLEANEX experiments [22], the results of which are shown in Fig. 4. Almost all of those backbone amides that exhibit relatively fast solvent exchange, ca. 1–10 s^{-1}, in aqueous solution (peaks in

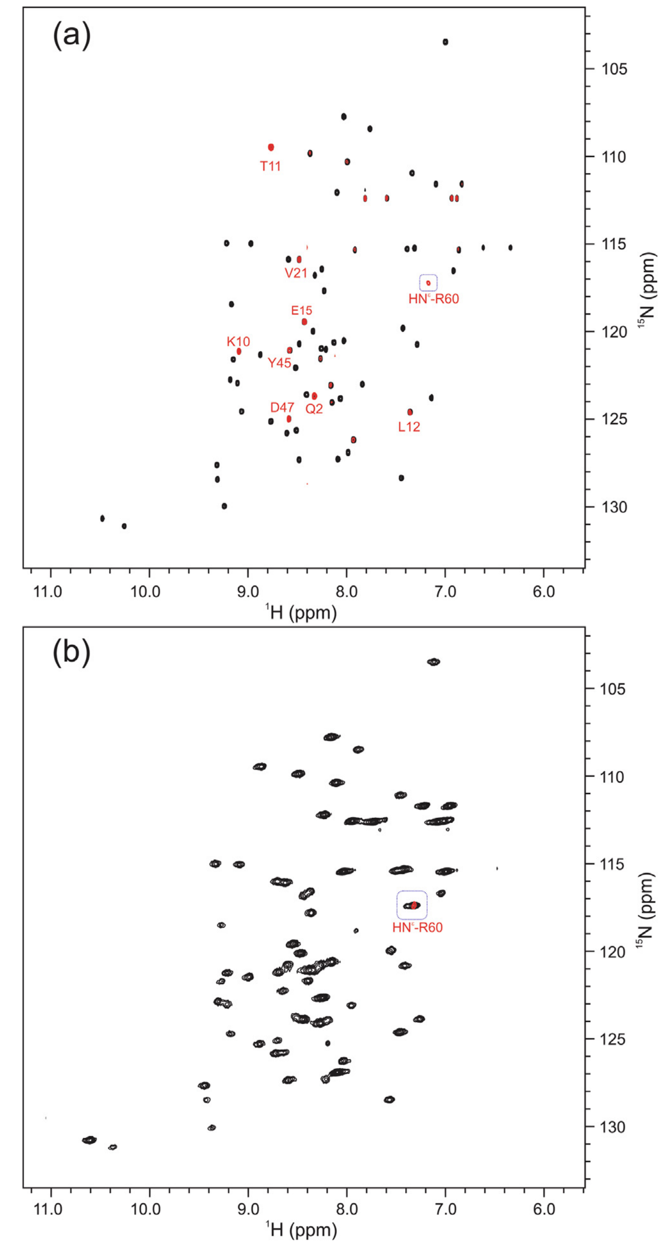

Fig. 4. Confirmation of reduced solvent-amide exchange between backbone amide protons of GB1 and solvent water in LCP. Overlay of ^{1}H-^{15}N HSQC spectrum (in black) and CLEANEX spectrum (τ_{mix} = 150 ms, in red) of GB1: (a) in aqueous solution; and (b) in LCP. Resonances that persist in the CLEANEX spectrum are labelled and are indicative of fast exchange (ca. 1 to 10 s^{-1}). (For interpretation of the references to colour in this figure legend, the reader is referred to the web version of this article.)

red, Fig. 4a), have their amide-solvent water exchange rates diminished upon LCP encapsulation with only the sidechain NH of Arg60 (Fig. 4b) giving rise to a cross peak in the CLEANEX experiments.

Finally, the abundant proton nuclear spins originating from the lipids, which contribute to substantial line broadening in the ^{1}H dimension (Fig. 3), potentially offer a rich "thermal bath" of spin magnetization (if their magnetizations are not perturbed) so as to speed up spectral acquisition of nuclear spins of interest, such as amides [23]. A comparison of the ^{1}H-^{15}N HSQC [24,25] and BEST ^{1}H-^{15}N HMQC spectra [26] acquired in aqueous solution and in LCP was carried out with the results presented in Fig. 5. The ratios of peak volume between BEST ^{1}H-^{15}N HMQC and non-selective conventional ^{1}H-^{15}N HSQC spectra for the backbone amides shown in Fig. 5 are listed in Table 1. Excluding the backbone amides undergoing rapid exchange with solvent water (such as Thr11), which gain extra sensitivity enhancement in aqueous solution [27], a widespread additional gain in sensitivity for backbone amides observed in BEST ^{1}H-^{15}N HMQC over non-selective conventional ^{1}H-^{15}N HSQC is clearly evident in LCP compared to the aqueous solution. For the parameters used in the present comparison, an average sensitivity gain of 2.33 (measured by peak volume ratios between ^{1}H-^{15}N BEST HMQC and non-selective conventional ^{1}H-^{15}N HSQC) in LCP versus 1.76 in aqueous solution was found. A residue by residue comparison in aqueous solution and LCP is presented in the Supplementary Material, Fig. S3. While this additional gain in spectral sensitivity is consistent with the presence of an abundant proton nuclear spin source attributed to the high lipid contents of the LCP, it is of particular significance given the absence of solvent water which serves as a 'thermal bath' of spin magnetization in aqueous solution. Although the current comparison was carried out using a BEST ^{1}H-^{15}N HMQC sequence, we expect comparable additional gains to be achievable with other forms of BEST-based RF pulse sequences, such as BEST ^{1}H-^{15}N HSQC and BEST triple-resonance sequences [28].

In conclusion, we have reported high resolution heteronuclear NMR correlation spectra of ^{15}N-enriched proteins encapsulated in a LCP matrix. Our results show LCP encapsulation: (1) does not introduce significant structural changes, (2) reduces solvent chemical exchange of backbone amides, and (3) offers additional spectral sensitivity gain with the use of band-selective excitation short-transient (BEST) spectroscopy. With the elimination of excessive bulk water, protein encapsulation in LCP provides a potential novel alternative to the use of reverse micelles, which involves the use of elevated pressure for protein encapsulation and dedicated low-viscosity fluids for the preparation of NMR samples [29,30], for the quantification of residue-specific hydration dynamics of proteins by NMR.

3. Experimental

3.1. Sample preparation

^{15}N-labelled B1 immunoglobulin-binding domain of Streptococcal protein (GB1) was prepared in an imidazole buffer with 50 mM imidazole and 10 mM $CaCl_2$ at pH 6.8 as described previously [31]. The protein was concentrated to ca. 1.8 mM in aqueous solution. The LCP samples containing ^{15}N-labelled GB1 were prepared by mixing aqueous GB1 solution (38% w/w) and molten monoolein (62% w/w) using a coupled syringe apparatus. Monoolein was purchased from Sigma-Aldrich (St Louis, MO). A needle was attached to the syringe and the LCP was injected into a 2 mm (o.d.) glass capillary, which was placed into a 5 mm NMR tube filled with ^2H_2O and fixed in place using a PTFE adapter. The sample was allowed to equilibrate for at least 12 h prior to NMR experiments.

3.2. NMR spectroscopy

All NMR spectra were acquired at 298.13 K on a Bruker Avance III 600 spectrometer equipped with a TCI cryoprobe fitted with a single-axis field gradient (*Gz*) and processed using TOPSPIN (Version 3.2, Bruker). The program XEASY (Version 1.4) was used for peak volume integration and confirmation of backbone assignments of GB1 [32]. Chemical shifts of ^{1}H were referenced to DSS at 0 ppm, and the ^{15}N chemical shifts were referenced indirectly using absolute frequency ratios [33]. All 2D ^{1}H-^{15}N HSQC, HMQC, and CLEANEX spectra presented in the current study were acquired with 1024 and 64 complex data points over spectral widths of 13.0

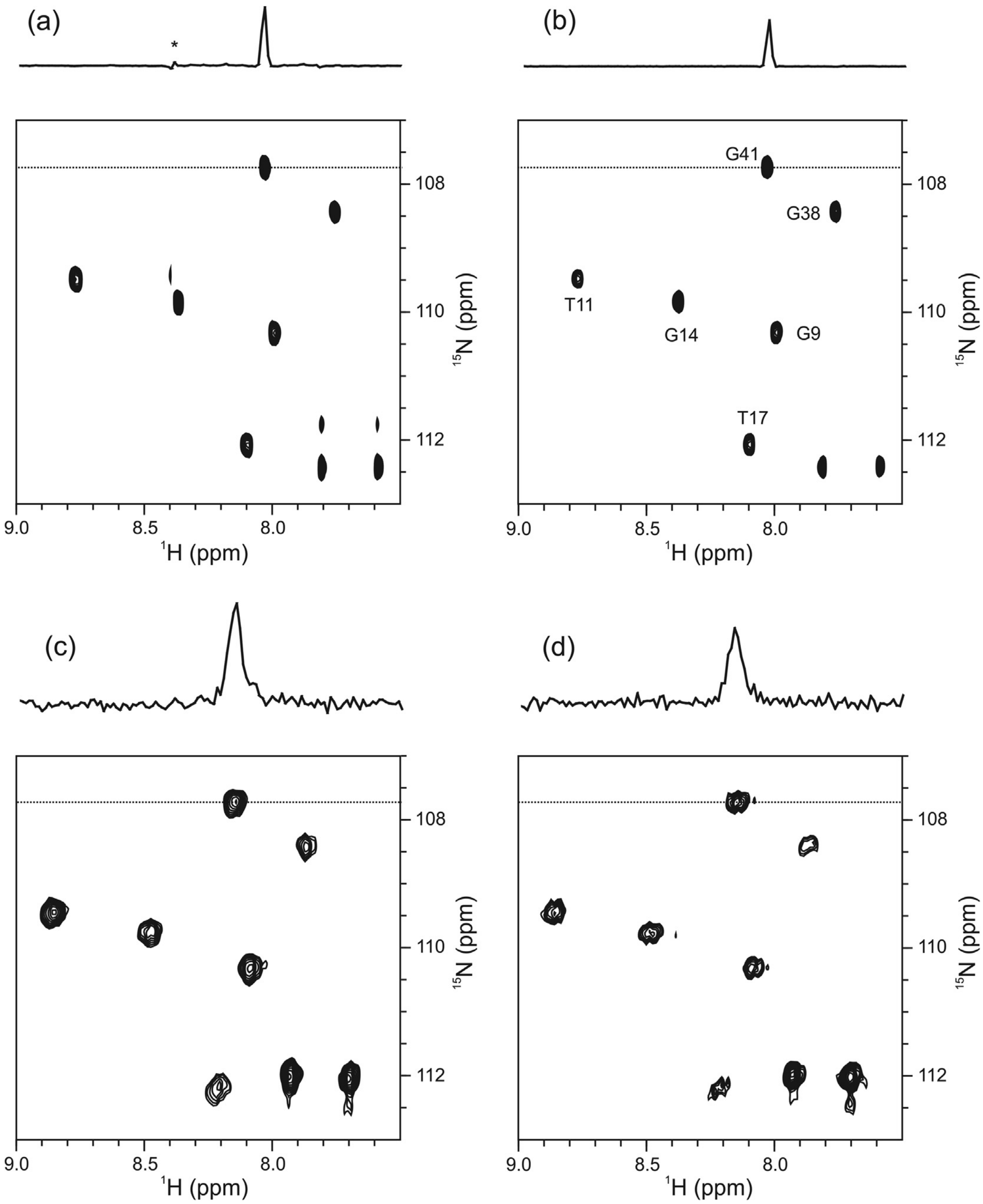

Fig. 5. Comparison of BEST ^{1}H-^{15}N HMQC and conventional (non-selective) ^{1}H-^{15}N HSQC spectra in LCP. Partial spectra of BEST ^{1}H-^{15}N HMQC (a, c) and conventional ^{1}H-^{15}N HSQC (b, d) of GB1, in aqueous solution and in LCP, respectively. One-dimensional traces of residue G41 extracted from the 2D spectra shown, after scaling to the same noise level via a spectral region where clearly no cross peaks were present, are depicted above each panel, respectively. For comparison, the total acquisition time was the same for BEST HMQC and conventional HSQC spectra, i.e., 2 h 40 min for spectra in LCP and 20 min in aqueous solution. For BEST HMQC, the relaxation delay was set at 0.359 s (including sampling time of 0.131 s) for LCP sample whereas for aqueous solution a value of 1.131 s was used. As a result, numbers of transients for signal averaging for BEST HMQC/HSQC were 192/64 in LCP and 24/8 in aqueous solution, respectively. All four spectra were processed with identical parameters, such as matrix size, applied window function and linear prediction in ^{15}N dimension (see Experimental Section for more details). It is worthwhile noting that the more noisy baselines as seen in 1D traces of (c) and (d) reflects the small amount of protein, 30 μL of GB1 at 1.8 mM, configured in this LCP sample. The small 'peak' at ca. 8.4 ppm, visible in the 1D trace above Fig. 5a (indicated with an asterisk) in aqueous solution arises from the intense signal of imidazole within the buffer solution and is more pronounced in the BEST HMQC than in the conventional HSQC spectrum (Fig. 5b).

and 32.0 ppm for ^{1}H and ^{15}N dimension, respectively. All datasets were linear predicted to 128 complex points in the ^{15}N dimension and a sine-bell shifted window function was used for both ^{1}H and ^{15}N dimensions. The dataset matrix after FT was 1024 by 1024 for all 2D spectra presented in the present study.

For the CLEANEX experiments, where a phase-modulated pulse train is applied to achieve a clean magnetization transfer exclusive to chemical exchange, were recorded using the standard CLEANEX-PM sequence (fhsqccxf3gpph, Bruker pulse sequence library) [22]. The selective RF pulse used for the inversion of water signal was a 7.5 ms Gaussian shaped-pulse. For the CLEANEX spectra shown in Fig. 4 (in red), an inter-scan delay of 2 s and the number of scans were 16 for aqueous solution (Fig. 4a) and 48 for LCP (Fig. 4b), respectively.

For the comparison of spectral sensitivity between BEST ^{1}H-^{15}N HMQC and non-selective conventional ^{1}H-^{15}N HSQC (Fig. 5), standard pulse sequences were used (hsqcetf3gpsi and sfhmqcf3gphph from Bruker pulse sequence library). For the BEST ^{1}H-^{15}N HMQC,

Table 1
Ratios of peak volumes between BEST ^{1}H-^{15}N HMQC and non-selective conventional ^{1}H-^{15}N HSQC spectra both in aqueous solution and in lipidic cubic phase (LCP).

Residues	Peak volume ratios[a]	
	In aqueous solution	In LCP
G9	1.71	2.30
T11	2.93	2.30
G14	1.85	1.91
T17	1.64	2.33
G38	1.60	2.18
G41	1.43	2.14

[a] To account for higher number of transients used for the acquisitions of BEST ^{1}H-^{15}N HMQC compared to non-selective conventional ^{1}H-^{15}N HSQC, BEST ^{1}H-^{15}N HMQC spectra both in aqueous solution and in LCPs were scaled to the same noise level via a spectral region where clearly no cross peaks were present as their respective ^{1}H-^{15}N HSQC spectra before integration of peak volumes.

the shaped pulse for ^{1}H excitation was a polychromatic PC9 of 3 ms with a rotation angle of 120°, and the subsequent band-selective ^{1}H refocusing pulse was an r-SNOB with duration of 1 ms as in the original sequence [26]. Offsets for both shaped-pulses PC9 and r-SNOB were 8.5 ppm.

Appendix A. Supplementary data

Supplementary data to this article can be found online at https://doi.org/10.1016/j.jmr.2019.06.017.

References

[1] B. Halle, Protein hydration dynamics in solution: a critical survey, Philos. T. R. Soc. B 359 (2004) 1207–1223.
[2] G. Otting, E. Liepinsh, K. Wuthrich, Protein hydration in aqueous-solution, Science 254 (1991) 974–980.
[3] K. Modig, E. Liepinsh, G. Otting, B. Halle, Dynamics of protein and peptide hydration, J. Am. Chem. Soc. 126 (2004) 102–114.
[4] N.V. Nucci, M.S. Pometun, A.J. Wand, Site-resolved measurement of water-protein interactions by solution NMR, Nat. Struct. Mol. Biol. 18 (2011) 245–249.
[5] N.V. Nucci, M.S. Pometun, A.J. Wand, Mapping the hydration dynamics of ubiquitin, J. Am. Chem. Soc. 133 (2011) 12326–12329.
[6] P.N. Gallo, J.C. Iovine, N.V. Nucci, Toward comprehensive measurement of protein hydration dynamics: facilitation of NMR-based methods by reverse micelle encapsulation, Methods 148 (2018) 146–153.
[7] V. Luzzati, A. Tardieu, T. Gulikkrzywicki, E. Rivas, Reisshus.F, Structure of cubic phases of lipid-water systems, Nature 220 (1968) 485–488.
[8] M. Caffrey, Membrane protein crystallization, J. Struct. Biol. 142 (2003) 108–132.
[9] T.G. Meikle, A. Zabara, L.J. Waddington, F. Separovic, C.J. Drummond, C.E. Conn, Incorporation of antimicrobial peptides in nanostructured lipid membrane mimetic bilayer cubosomes, Colloid Surf. B 152 (2017) 143–151.
[10] J.C. Shah, Y. Sadhale, D.M. Chilukuri, Cubic phase gels as drug delivery systems, Adv. Drug Deliver. Rev. 47 (2001) 229–250.
[11] X. Mulet, B.J. Boyd, C.J. Drummond, Advances in drug delivery and medical imaging using colloidal lyotropic liquid crystalline dispersions, J. Colloid Interf. Sci. 393 (2013) 1–20.
[12] S. Sarkar, N. Tran, M.H. Rashid, T.C. Le, I. Yarovsky, C.E. Conn, C.J. Drummond, Toward cell membrane biomimetic lipidic cubic phases: a high-throughput exploration of lipid compositional space, ACS Appl. Bio Mater. 2 (2018) 182–195.
[13] L. van't Hag, S.L. Gras, C.E. Conn, C.J. Drummond, Lyotropic liquid crystal engineering moving beyond binary compositional space–ordered nanostructured amphiphile self-assembly materials by design, Chem. Soc. Rev. 46 (2017) 2705–2731.
[14] L. Van't Hag, C. Darmanin, T.C. Le, S. Mudie, C.E. Conn, C.J. Drummond, In meso crystallization: compatibility of different lipid bicontinuous cubic mesophases with the cubic crystallization screen in aqueous solution, Cryst. Growth Des. 14 (2014) 1771–1781.
[15] V. Cherezov, H. Fersi, M. Caffrey, Crystallization screens: Compatibility with the lipidic cubic phase for in meso crystallization of membrane proteins, Biophys. J. 81 (2001) 225–242.
[16] C.E. Conn, C. Darmanin, X. Mulet, A. Hawley, C.J. Drummond, Effect of lipid architecture on cubic phase susceptibility to crystallisation screens, Soft Matter 8 (2012) 6884–6896.
[17] C. Darmanin, C.E. Conn, J. Newman, X. Mulet, S.A. Seabrook, Y.L. Liang, A. Hawley, N. Kirby, J.N. Varghese, C.J. Drummond, High-throughput production and structural characterization of libraries of self-assembly lipidic cubic phase materials, ACS Comb. Sci. 14 (2012) 247–252.
[18] W. Liu, M. Caffrey, Gramicidin structure and disposition in highly curved membranes, J. Struct. Biol. 150 (2005) 23–40.
[19] E. Boyle-Roden, N. Hoefer, K.K. Dey, P.J. Grandinetti, M. Caffrey, High resolution HNMR of a lipid cubic phase using a solution NMR probe, J. Magn. Reson. 189 (2007) 13–19.
[20] T.S. Ulmer, I.D. Campbell, J. Boyd, Amide proton relaxation measurements employing a highly deuterated protein, J. Magn. Reson. 166 (2004) 190–201.
[21] M. Sattler, S.W. Fesik, Use of deuterium labeling in NMR: Overcoming a sizeable problem, Structure 4 (1996) 1245–1249.
[22] T.L. Hwang, P.C.M. van Zijl, S. Mori, Accurate quantitation of water-amide proton exchange rates using the phase-modulated CLEAN chemical EXchange (CLEANEX-PM) approach with a Fast-HSQC (FHSQC) detection scheme, J. Biomol. NMR 11 (1998) 221–226.
[23] M. Deschamps, I.D. Campbell, Cooling overall spin temperature: protein NMR experiments optimized for longitudinal relaxation effects, J. Magn. Reson. 178 (2006) 206–211.
[24] A.G. Palmer, J. Cavanagh, P.E. Wright, M. Rance, Sensitivity improvement in proton-detected 2-dimensional heteronuclear correlation NMR-spectroscopy, J. Magn. Reson. 93 (1991) 151–170.
[25] S. Grzesiek, A. Bax, The importance of not saturating H_2O in protein NMR - Application to sensitivity enhancement and NOE measurements, J. Am. Chem. Soc. 115 (1993) 12593–12594.
[26] P. Schanda, B. Brutscher, Very fast two-dimensional NMR spectroscopy for real-time investigation of dynamic events in proteins on the time scale of seconds, J. Am. Chem. Soc. 127 (2005) 8014–8015.
[27] S. Yao, M.G. Hinds, J.M. Murphy, R.S. Norton, Exchange enhanced sensitivity gain for solvent-exchangeable protons in 2D ^{1}H–^{15}N heteronuclear correlation spectra acquired with band-selective pulses, J. Magn. Reson. 211 (2011) 243–247.
[28] E. Lescop, P. Schanda, B. Brutscher, A set of BEST triple-resonance experiments for time-optimized protein resonance assignment, J. Magn. Reson. 187 (2007) 163–169.
[29] R.W. Peterson, N.V. Nucci, A.J. Wand, Modification of encapsulation pressure of reverse micelles in liquid ethane, J. Magn. Reson. 212 (2011) 229–233.
[30] N.V. Nucci, K.G. Valentine, A.J. Wand, High-resolution NMR spectroscopy of encapsulated proteins dissolved in low-viscosity fluids, J. Magn. Reson. 241 (2014) 137–147.
[31] A. Sethi, S. Bruell, N. Patil, M.A. Hossain, D.J. Scott, E.J. Petrie, R.A.D. Bathgate, P. R. Gooley, The complex binding mode of the peptide hormone H2 relaxin to its receptor RXFP1, Nat. Commun. 7 (2016).
[32] C. Bartels, T.H. Xia, M. Billeter, P. Güntert, K. Wüthrich, The program XEASY for computer-supported NMR spectral-analysis of biological macromolecules, J. Biomol. NMR 6 (1995) 1–10.
[33] D.S. Wishart, C.G. Bigam, J. Yao, F. Abildgaard, H.J. Dyson, E. Oldfield, J.L. Markley, B.D. Sykes, ^{1}H, ^{13}C and ^{15}N chemical shift referencing in biomolecular NMR, J. Biomol. NMR 6 (1995) 135–140.